Bi-level Supply Restoration Method for Active Distribution Networks Considering Multi-resource Coordination

Guanyu Song, *Senior Member*, *IEEE*, Chiyuan Ma, Haoran Ji, *Senior Member*, *IEEE*, Hany M. Hasanien, *Senior Member*, *IEEE*, Jiancheng Yu, Jinli Zhao, *Member*, *IEEE*, Hao Yu, *Senior Member*, *IEEE*, and Peng Li, *Senior Member*, *IEEE*

***Abstract*—The volatility of increasing distributed generators (DGs) poses a severe challenge to the supply restoration of active distribution networks (ADNs). The integration of power electronic devices represented by soft open points (SOPs) and mobile energy storages (MESs) provides a promising opportunity for rapid supply restoration with high DG penetration. Oriented for the post-event rapid restoration of ADNs, a bi-level supply restoration method is proposed considering the multi-resource coordination of switches, SOPs, and MESs. At the upper level (long-timescale), a multi-stage supply restoration model is developed for multiple resources under uncertainties of DGs and loads. At the lower level (short-timescale), a rolling correction restoration strategy is proposed to adapt to the DG and load fluctuations on short timescales. Finally, the effectiveness of the proposed method is verified based on a modified practical distribution network and IEEE 123-node distribution network. Results show that the proposed method can fully utilize the coordination potential of multiple resources to improve load restoration ratio for ADNs with DG uncertainties.**

***Index Terms*—Active distribution network (ADN), soft open point (SOP), distributed generator (DG), supply restoration, mobile energy storage (MES), uncertainty, multi-resource coordination.**

I. Introduction

DISTRIBUTION networks play a crucial role in the power supply for users, necessitating high reliability. Therefore, it is crucial to realize the rapid post-event supply restoration of distribution networks [1]. With the integration of distributed generators (DGs) such as wind turbines and photovoltaics, distribution networks have evolved into active distribution networks (ADNs) [2]. However, the volatility and uncertainty of DGs pose severe challenges to rapid supply restoration [3].

The integration of power electronic devices represented by soft open points (SOPs) and mobile energy storages (MESs) provides a promising opportunity for rapid supply restoration with high penetration of DGs. ADNs provide voltage and power support to outage regions by intelligently switching control modes of flexible resources, providing an opportunity for rapid post-event restoration with high penetration of DGs [4].

SOPs, which replace traditional tie switches, play an important role in ADNs [5]. Composed of fully controlled power electronic devices, SOPs can quickly and accurately control power flow to achieve the joint adjustment of active and reactive power [6]. The application of SOPs possesses great potential for enhancing DG consumption [7], balancing feeder loads, and rapid supply restoration [8]. It is significant to study the restoration strategy of SOPs in ADNs.

Supply restoration methods for ADNs based on SOPs have been extensively studied. A bi-level interval robust optimization model was proposed in [9] to improve the efficiency of supply restoration. Reference [10] proposed a supply restoration method that fully exploited the potential benefits of multiple SOPs. Reference [11] proposed a multiple-source distribution restoration strategy considering SOPs to enhance the load restoration level of ADNs. The above research works primarily focused on the power transfer capability of SOPs in the spatial dimension. The storage of energy in the temporal dimension needs further research [12].

The integration of flexible resources into DC link has also been investigated to improve the regulatory capability of SOPs. Reference [13] proposed a robust operation method to improve the economy of electric vehicles (EVs) and flexibility of ADN. An energy storage system (ESS) was connected to the DC link of SOP to enhance its power supply capacity in [14]. Compared with SOPs, mobile emergency generators enable the transfer of energy in the temporal dimension. Based on the truck-mounted modular structure, mobile emergency generators can realize energy transfer among nodes at

Manuscript received: June 13, 2024; revised: October 18, 2024; accepted: December 17, 2024. Date of CrossCheck: December 17, 2024. Date of online publication: January 20, 2025.

This work was supported in part by the National Natural Science Foundation of China (No. U22B20114) and Guizhou Provincial Science and Technology Projects (No. [2023] General 292).

G. Song, C. Ma, H. Ji (corresponding author), J. Zhao, H. Yu, and P. Li are with the Key Laboratory of Smart Grid of Ministry of Education, Tianjin University, Tianjin, China (e-mail: gysong@tju. edu. cn; mcy_1@tju. edu. cn; jihaoran@tju.edu.cn; jlzhao@tju.edu.cn; tjuyh@tju.edu.cn; lip@tju.edu.cn).

H. M. Hasanien is with the Faculty of Engineering, Ain Shams University, Cairo, Egypt, and he is also with the Faculty of Engineering and Technology, Future University in Egypt, Cairo, Egypt (e-mail: hanyhasanien@ieee.org).

J. Yu is with the State Grid Tianjin Electric Power Company, Tianjin, China (e-mail: yujiancheng@126.com).

DOI: 10.35833/MPCE.2024.000616

different locations and operate more flexibly [15]. However, due to the congestion and other traffic conditions, the mobility efficiency is relatively low. Hence, the coordination of mobile emergency generators and SOPs is of great significance for enhancing the restoration capability of the ADNs.

Traditional mobile emergency generators (e.g., mobile diesel generators) can be connected to the grid via AC modular to provide energy to the outage regions. Reference [16] proposed a pre-disaster allocation method of mobile emergency generators and electric buses in urban power networks to reduce the expected cost of load loss. A three-stage planning method considered the integration of mobile diesel generators and mobile energy storages to improve the resilience of microgrids in [17]. However, after restoration, the diesel generators can only discharge to ADNs [18]. The excess energy generated by DGs may not be fully utilized. Compared with mobile diesel generators, MESs can also absorb excess energy to achieve peak shaving and valley filling in ADNs. Moreover, MESs can supply power to the feeders connected to both terminals of SOP simultaneously via the DC link, thereby enhancing the supply restoration capability.

There are extensive research works on the operational optimization strategies for MESs in ADNs. A two-step optimal allocation model is proposed to achieve the optimal allocation of MESs and reduce the annual cost of ADNs in [19]. Reference [20] proposed a multi-stage robust optimization model considering MES flexibility to reduce system operation costs. Reference [21] proposed a rolling restoration strategy based on MESs to improve the load restoration ratio. Thus, the flexibility of SOP can be further enhanced by integrating MESs into the DC link of SOP. Nevertheless, existing research works on SOP with the integration of flexible resources mainly focused on reducing the operation costs of ADNs under normal conditions. Further research on SOP with the integration of MES is required to improve the restoration level of ADNs under fault conditions.

Supply restoration with multi-resource coordination has been investigated to fully exploit the potential of flexible resources. Reference [22] proposed a co-optimization model to route repair crews and MESs for supply restoration in distribution networks. A decision-making method was proposed in [23] to derive the restoration strategy coordinating multiple sources for critical load restoration. Reference [24] proposed a restoration scheme to maximize restored weighted loads based on the coordination of ESSs, DGs, and MESs. In [25], a coordinated restoration method was proposed to enhance the resilience of hybrid AC/DC distribution network. As different devices operate on different timescales, the operation sequence would affect the effectiveness of the restoration strategy. Hence, the multi-timescale characteristics of devices need to be further explored to coordinate the operation sequence.

The multi-stage concept has been introduced to achieve the coordination of multiple types of resources on multiple timescales. Reference [26] proposed a power supply restoration method with multiple fixed time steps to generate an optimal action sequence for multiple types of resources. Reference [27] proposed a dynamic supply restoration model with variable time steps to achieve coordination between manually and remotely controlled switches. A multi-step reconfiguration model to achieve sequential switch actions and DG operations over the entire restoration horizon was formulated in [28]. Reference [29] considered the coordination of SOPs and multiple types of switches to further improve supply restoration efficiency. However, the uncertainties and fluctuations of DGs and loads have a significant impact on ADNs [30]. The variability of traffic information also affects the effectiveness of MES scheduling strategies. An investigation of rolling correction restoration strategy is necessary to reduce the impact of uncertainties.

To address these problems, a bi-level supply restoration method for ADNs that considers multi-resource coordination is proposed, as shown in Fig. 1. At the upper level, a multi-stage supply restoration model with the uncertainty of DGs and loads is developed to derive strategies of switch operation and selection of SOP control mode on long timescales. To deal with the fluctuations of DGs and traffic conditions, a rolling correction restoration strategy is proposed at the lower level on short timescales. The proposed method coordinates the operation strategies of multiple resources on multi-timescale to improve the level of ADN restoration. In Fig. 1, the blue number line represents the minimum time interval; the green arrows indicate the duration of each stage on a long timescale; and the orange arrows represent the rolling correction timescale at the lower level. Based on the predicted and updated information of multiple types of loads, the restoration strategies at the upper and lower levels can be derived separately.

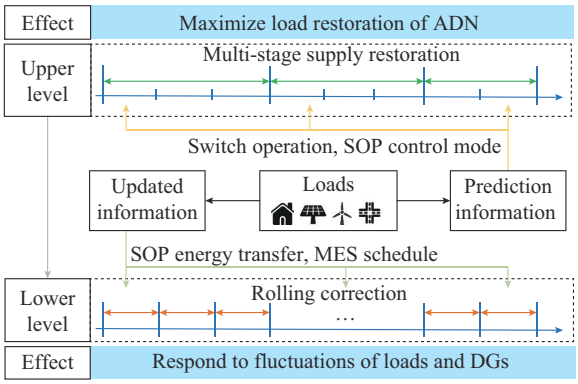

Fig. 1. Schematic of proposed bi-level supply restoration method for ADNs.

The main contributions are summarized as follows.

1) A bi-level supply restoration method of multi-terminal SOP with MES integration is proposed. The SOP mode is selected to ensure the coordination with MESs in ADNs.

2) At the upper level, a multi-stage supply restoration model with uncertainty of DGs and loads is developed for multiple resources. The strategies of switch operation and selection of SOP control mode considering the uncertainties of DGs and loads are determined to maximize load restoration on a long timescale.

3) At the lower level, a rolling correction restoration strategy is proposed for supply restoration of ADN. The power outputs of SOPs and MESs are corrected to adapt to DG and

load fluctuations and varied traffic conditions, thereby improving the efficiency of short-timescale supply restoration.

The remainder of this paper is organized as follows. In Section II, the bi-level supply restoration method of multi-terminal SOP with MES integration is developed. Section III proposes a multi-stage supply restoration model at the upper level. A rolling correction restoration strategy at the lower level is proposed in Section IV. Case studies on a modified practical distribution network are presented in Section V. Finally, conclusion is given in Section VI.

II. Bi-level Supply Restoration Method of Multi-terminal SOP with MES Integration

In this section, the bi-level supply restoration method of multi-terminal SOP with MES integration is proposed to achieve the coordination between SOP and MES. Considering the impact of the peak intervals of the transport network, the MES operation model is modified to ensure the effectiveness of the proposed method.

A. Bi-level Supply Restoration Method with MES Integration

Based on a fully-controlled voltage source converter (VSC), each SOP terminal can be operated with multiple control modes. The SOP control method without MES integration has been analyzed in [31]. The control modes of SOP with MES integration in fault scenarios are presented in Table I.

TABLE I
Control Modes of SOP with MES Integration in Fault Scenarios

Fault scenario	Control mode	
	VSC 1	VSC 2
Fault on VSC 1 side	$U_{ac}\theta$	$U_{dc}Q/U_{dc}U_{ac}$
Fault on VSC 2 side	$U_{dc}Q/U_{dc}U_{ac}$	$U_{ac}\theta$
Faults on both sides	$U_{ac}\theta$	$U_{ac}\theta$

As presented in Table I, the control mode of the SOP terminal located in the outage region switches to $U_{ac}\theta$ control mode to provide voltage support. When both sides are located in outage regions simultaneously, MES can provide power to both terminals. In this case, VSC 1 and VSC 2 adopt $U_{ac}\theta$ control mode to provide voltage support for each outage region, as shown in Fig. 2.

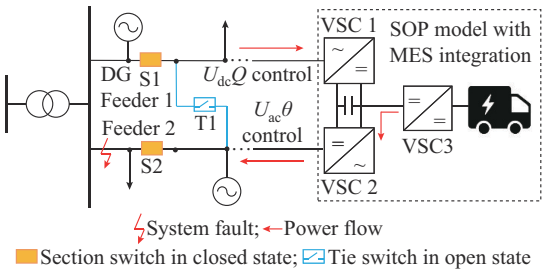

Fig. 2. Schematic of control modes of SOP terminals under faults.

As can be seen in Fig. 2, when a fault occurs on Feeder 2, the SOP quickly locks to isolate the short-circuit current. The corresponding protective devices are activated to achieve rapid isolation of the fault. After that, the SOP control strategy quickly switches to transfer power from Feeder 1 to Feeder 2. VSC 2 uses the $U_{ac}\theta$ control mode to provide voltage support to the fault region, and VSC 1 adopts the $U_{dc}Q$ control mode to provide power support for rapid restoration. The direction of power flow is indicated by the red arrows. When there is no SOP, the tie switch T1 operates to transfer power to the fault region. However, tie switches cannot ensure the voltage quality after restoration, which may lead to low restoration ratios in the fault regions.

Based on the above analysis, the restoration method of multi-terminal SOP with MES integration is modeled as:

$$0 \le Z_{i,t} + Z_{j,t} \le 1 + \sum_{m \in \Omega_M} \alpha_{n,m,t} \quad \forall i,j \in \Omega_{SOP}, n \in \Omega_R \tag{1a}$$

$$v_{i,t} - U_0^2 \ge -M\left(1 - Z_{i,t}\right) \quad i \in \Omega_{SOP} \tag{1b}$$

where Ω_M and Ω_{SOP} are the sets of MESs and nodes with SOP terminals, respectively; Ω_R is the set of MES integration points; $Z_{i,t}$ and $Z_{j,t}$ indicate whether the SOP terminal provides voltage support in time interval t; $\alpha_{n,m,t}$ is the binary variable indicating the integration status of MES m at the DC link n of SOP in time interval t; $v_{i,t}$ and U_0^2 are the voltage square of node i in time interval t and the voltage reference square value, respectively; and M is a large constant for modeling.

Equation (1a) indicates that if no MES is integrated into the SOP, only one terminal can provide voltage support to the outage region. The SOP terminal with $U_{ac}\theta$ control mode maintains the voltage of its connected node no less than U_0, as shown in (1b). The modified SOP operation constraints with MES integration are given by:

$$P_{i,t}^{SOP} + P_{j,t}^{SOP} + P_{i,t}^{SOP,L} + P_{j,t}^{SOP,L} - \sum_{m \in \Omega_M} \left(P_{n,m,t} + P_{n,m,t}^{MES,L}\right) = 0$$
$$\forall i,j \in \Omega_{SOP}, n \in \Omega_R, m \in \Omega_M \tag{2a}$$

$$P_{n,m,t}^{MES,L} = \left|P_{n,m,t}\right| A_n \quad \forall n \in \Omega_R, m \in \Omega_M \tag{2b}$$

$$\left\| \left[P_{i,t}^{SOP} \quad Q_{i,t}^{SOP}\right]^T \right\|_2 \le \frac{P_{i,t}^{SOP,L}}{A_i} \tag{2c}$$

$$\left\| \left[P_{i,t}^{SOP} \quad Q_{i,t}^{SOP}\right]^T \right\|_2 \le S_{i,\max} \tag{2d}$$

$$P_{i,\min} \le P_{i,t}^{SOP} \le P_{i,\max} \tag{2e}$$

$$Q_{i,\min} \le Q_{i,t}^{SOP} \le Q_{i,\max} \tag{2f}$$

where $P_{i,t}^{SOP}$ and $Q_{i,t}^{SOP}$ are the active and reactive power outputs of SOP at node i in time interval t, respectively; $P_{n,m,t}$ is the active power output of MES m in time interval t; $P_{i,t}^{SOP,L}$ and $P_{n,m,t}^{MES,L}$ are the active power losses of SOP at node i and MES m in time interval t; A_i, A_j, and A_n are the loss coefficients of SOP terminals, respectively; $P_{i,\min}$ and $P_{i,\max}$ are the minimum and maximum active power outputs of SOP, respectively; $Q_{i,\min}$ and $Q_{i,\max}$ are the minimum and maximum reactive power outputs of SOP, respectively; and $S_{i,\max}$ is the maximum capacity of SOP.

The power transfer constraint among the terminals of SOP is denoted by (2a) with MES integration. Equations (2b) and (2c) represent the losses of MES and SOP, respectively. The

capacity of the terminals of SOP is constrained by (2d) and (2f). Meanwhile, (2b) can be linearized by (3a) and (3b):

$$P_{n,m,t}^{\mathrm{MES,L}} \geq P_{n,m,t} A_n \quad \forall n \in \Omega_{\mathrm{R}}, m \in \Omega_{\mathrm{M}} \tag{3a}$$

$$P_{n,m,t}^{\mathrm{MES,L}} \geq -P_{n,m,t} A_n \quad \forall n \in \Omega_{\mathrm{R}}, m \in \Omega_{\mathrm{M}} \tag{3b}$$

B. MES Operation Model Considering Traffic Conditions

The MES operation model includes the charging/discharging and mobility constraints [32], [33].

1) Charging/discharging Constraints

$$-\alpha_{n,m,t} P^{\mathrm{N}} \leq P_{n,m,t} \leq \alpha_{n,m,t} P^{\mathrm{N}} \quad \forall n \in \Omega_{\mathrm{R}}, m \in \Omega_{\mathrm{M}} \tag{4a}$$

$$\alpha_{n,m,t} \in \{0,1\} \tag{4b}$$

$$E_{m,t+1} = E_{m,t} - P_{n,m,t} \Delta t - \gamma_{m,t} \varepsilon v \Delta t \tag{4c}$$

$$\gamma_{m,t} \in \{0,1\} \tag{4d}$$

$$E_{m,\min} \leq E_{m,t} \leq E_{m,\max} \tag{4e}$$

where P^{N} is the rated power of MES; $E_{m,t}$ is the state of charge (SOC) of MES m in time interval t; $\gamma_{m,t}$ is the binary variable indicating the travelling status of MES m in time interval t; ε is the MES power consumption per unit distance; v is the speed of the MES; Δt is the unit time interval; and $E_{m,\min}$ and $E_{m,\max}$ are the minimum and maximum SOCs of MES m, respectively.

Equations (4a) and (4b) indicate that MES can interact with ADN only if integrated into the DC link of SOP. The state of charge (SOC) constraints of MES are represented in (4c)-(4e).

2) Mobility Constraints

$$\alpha_{\delta_m,m,0} = 1 \quad \forall m \in \Omega_{\mathrm{M}} \tag{5a}$$

$$\sum_{m \in \Omega_{\mathrm{M}}} \alpha_{i,m,t} \leq C \quad \forall i \in \Omega_{\mathrm{R}} \tag{5b}$$

$$\gamma_{m,t} + \sum_{i \in \Omega_{\mathrm{R}}} \alpha_{i,m,t} = 1 \tag{5c}$$

$$\sum_{\tau=t+1}^{\min\left(t+\Gamma_{ij,t},\, T\right)} \alpha_{j,m,t} \leq \left(1-\alpha_{i,m,t}\right) \min\left(\Gamma_{ij,t}, T-t\right) \quad \forall i,j \in \Omega_{\mathrm{R}} \tag{5d}$$

where δ_m is the initial position of MES m; C is the maximum number of MESs connected; $\Gamma_{ij,t}$ is the travelling time from node i to node j in time interval t; and T is the number of time intervals in the operating cycle.

Equation (5a) shows the initial positions of MESs. Equation (5b) constrains the maximum number C of MESs integrated into SOP. Equation (5c) indicates that MESs can be integrated into at most one SOP in each time interval. Equation (5d) ensures that MESs have sufficient travelling time among SOPs.

Additionally, the peak and off-peak intervals of the transport network affect the MES scheduling strategies. The travelling time of the MES is modified by:

$$\Gamma_{ij,t} = \begin{cases} \min\left(T_{ij,t}^{\mathrm{H}}, T_{ij,t}^{\mathrm{L}} + \left(1 - \dfrac{T_{ij,t}^{\mathrm{L}}}{T_{ij,t}^{\mathrm{H}}}\right)\left(T_{\mathrm{L}} - t\right)\right) & t \in \Omega_{\mathrm{T}}^{\mathrm{H}} \\ \max\left(T_{ij,t}^{\mathrm{L}}, T_{ij,t}^{\mathrm{H}} + \left(1 - \dfrac{T_{ij,t}^{\mathrm{H}}}{T_{ij,t}^{\mathrm{L}}}\right)\left(T_{\mathrm{H}} - t\right)\right) & t \in \Omega_{\mathrm{T}}^{\mathrm{L}} \end{cases} \tag{6}$$

where $T_{ij,t}^{\mathrm{H}}$ and $T_{ij,t}^{\mathrm{L}}$ are the travelling time of MESs in peak and off-peak time intervals of transport network, respectively, which can be obtained by Dijkstra algorithm; T_{H} and T_{L} are the start-of-the-peak and off-peak time intervals, respectively; and $\Omega_{\mathrm{T}}^{\mathrm{H}}$ and $\Omega_{\mathrm{T}}^{\mathrm{L}}$ are the sets of peak and off-peak time intervals, respectively.

III. Multi-stage Supply Restoration Model at Upper Level

In this section, the multi-stage supply restoration model of ADN is formulated at the upper level. Considering the uncertainties of DGs and loads, the strategies of switch operation and the selection of SOP control mode are obtained.

A. Stage Division Method

Before stage division, the ADN is divided into several regions based on the positions of faults and switches to reduce the number of binary variables. The regional division method is described in [29]. Furthermore, the energized status $E_{k,s}$ is defined to indicate whether regions are energized or not, as shown in (7a)-(7d).

$$\sum_{i \in \pi(k)} F_{ik,s} - \sum_{j \in \xi(k)} F_{kj,s} \leq E_{k,s} + M Z_{r,s} \quad r \in \Omega_k \bigcap \Omega_{\mathrm{F}} \tag{7a}$$

$$\sum_{i \in \pi(k)} F_{ik,s} - \sum_{j \in \xi(k)} F_{kj,s} \leq E_{k,s} + M Z_{r,s} \quad r \in \Omega_k \bigcap \Omega_{\mathrm{F}} \tag{7b}$$

$$-M s_{ij,s} \leq F_{ij,s} \leq M s_{ij,s} \quad ij \in \Omega_{\mathrm{L}}^{\mathrm{sw}} \tag{7c}$$

$$Z_{r,s} = 0 \quad r \in \Omega_{\mathrm{B}} \backslash \left(\Omega_{\mathrm{SOP}} \bigcup \Omega_{\mathrm{G}}\right) \tag{7d}$$

where Ω_k is the set of nodes in region k; Ω_{F} is the set of candidate fictitious source nodes; $\Omega_{\mathrm{L}}^{\mathrm{sw}}$ is the set of switches; Ω_{B} and Ω_{G} are the sets of all nodes and substations, respectively; $\pi(k)$ and $\xi(k)$ are the upstream and downstream regions of region k, respectively; $E_{k,s}$ is the binary variable indicating energized status of region k at stage s; $F_{ik,s}$ and $F_{kj,s}$ are the fictitious flow variables of line ik and kj at stage s, respectively, for the energized status constraints; $Z_{r,s}$ indicates whether the node r located in region k provides voltage support at stage s; and $s_{ij,s}$ is the binary variable indicating the status of switch ij at stage s.

Equations (7a) and (7b) represent that the outage regions can be energized by switches and SOPs. Equation (7c) indicates that when the switch is on, no fictitious flow can be provided to the outage regions. Equation (7d) denotes that nodes without connecting SOPs cannot actively provide voltage support to the ADN. The nodes in the energized regions can be restored.

As indicated in (7a)-(7d), the energized status of outage regions is related to switch status and SOP control mode. Considering the slow action of switches, the supply restoration process is divided into several stages based on switch operation intervals. The time-stage mapping constraints are given by:

$$\begin{cases} \sum_{s \in \Omega_{\mathrm{S}}} K_{t,s} = 1 \\ T_s - M\left(1 - K_{t,s}\right) \leq t \leq T_{s+1} + M\left(1 - K_{t,s}\right) \end{cases} \quad \forall t, s \tag{8a}$$

$$T_s - T_{s-1} \geq \left| s_{ij,s} - s_{ij,s-1} \right| T_{ij} \quad \forall ij \in \Omega_{\mathrm{L}}^{\mathrm{sw}} \tag{8b}$$

where Ω_{S} is the set of restoration stages; $K_{t,s}$ is the binary variable indicating whether time interval t is related to stage s; T_s is the starting time of stage s; and T_{ij} is the operation time of switches ij.

Equation (8a) denotes that each time interval t is related to a specific restoration stage. Equation (8b) ensures that the duration of each stage satisfies the required time intervals of switch operation.

B. Multi-stage Supply Restoration Model of ADN

A multi-stage supply restoration model is established with coordinated operation of flexible devices.

1) Objective Function for Supply Restoration

The objective function f of the multi-stage supply restoration model is given by:

$$\min f = f_{\mathrm{P}} + f_{\mathrm{L}} + f_{\mathrm{E}} + f_{\mathrm{S}} \tag{9a}$$

$$f_{\mathrm{P}} = c_{\mathrm{P}} \sum_{t \in \Omega_{\mathrm{T}}} \sum_{i \in \Omega_{\mathrm{B}}} \left(1 - R_{i,t}\right) P_{i,t}^{\mathrm{LOAD}} \Delta t \tag{9b}$$

$$f_{\mathrm{L}} = c_{\mathrm{L}} \sum_{t \in \Omega_{\mathrm{T}}} \sum_{ij \in \Omega_{\mathrm{L}}} r_{ij} l_{ij,t} \Delta t \tag{9c}$$

$$f_{\mathrm{E}} = c_{\mathrm{L}} \sum_{t \in \Omega_{\mathrm{T}}} \left(\sum_{i \in \Omega_{\mathrm{SOP}}} P_{i,t}^{\mathrm{SOP,L}} + \sum_{n \in \Omega_{\mathrm{R}}} \sum_{m \in \Omega_{\mathrm{M}}} P_{n,m,t}^{\mathrm{MES,L}} + \sum_{m \in \Omega_{\mathrm{M}}} \gamma_{m,t} \varepsilon v \right) \Delta t \tag{9d}$$

$$f_{\mathrm{S}} = c_{\mathrm{S}} \sum_{s \in \Omega_{\mathrm{S}}} \sum_{ij \in \Omega_{\mathrm{L}}^{\mathrm{sw}}} \left| s_{ij,s} - s_{ij,s-1} \right| \tag{9e}$$

where Ω_{T} and Ω_{L} are the sets of time intervals and lines, respectively; f_{P} is the cost of the unrestored load; f_{L} is the cost of power loss; f_{E} is the flexible resource operation cost; f_{S} is the operation cost of switching action; $R_{i,t}$ is the restoration ratio of each node in time interval t; c_{P}, c_{L}, and c_{S} are the unit prices of load loss, power purchasing, and switch operation, respectively; r_{ij} is the resistance of line ij; and $l_{ij,t}$ is the current square of line ij in time interval t.

The total cost during the supply restoration of ADN is represented by (9a). Equation (9b) denotes the penalty cost of unrestored load. In addition to the unrestored load cost, the cost of network losses and the operation costs of multiple resources should be considered, which are indicated by (9c)-(9e). Since the focus of the restoration method is to minimize the active power of unrestored loads, c_{P} is required to be significantly larger than the other cost factors.

2) Operation Constraints of ADN

The modified fictitious flow constraints are adopted to ensure the radial operation of ADN, as shown in (10a)-(10h).

$$\sum_{ij \in \Omega_{\mathrm{L}}^{\mathrm{sw}}} s_{ij,s} = N_{\mathrm{Z}} + N_{\mathrm{G}} - \sum_{r \in \Omega_{\mathrm{F}}} \lambda_{r,s} \quad ij \in \Omega_{\mathrm{L}}^{\mathrm{sw}} \tag{10a}$$

$$\lambda_{r,s} = 1 \quad r \in \Omega_{\mathrm{G}} \tag{10b}$$

$$s_{ij,s} \in \{0,1\} \quad ij \in \Omega_{\mathrm{L}}^{\mathrm{sw}} \tag{10c}$$

$$-M s_{ij,s} \leq f_{ij,s} \leq M s_{ij,s} \quad ij \in \Omega_{\mathrm{L}}^{\mathrm{sw}} \tag{10d}$$

$$\sum_{i \in \pi(k)} f_{ik,s} - \sum_{j \in \xi(k)} f_{kj,s} \leq 1 + M\lambda_{r,s} \quad r \in \Omega_k \cap \Omega_{\mathrm{F}} \tag{10e}$$

$$\sum_{i \in \pi(k)} f_{ik,s} - \sum_{j \in \xi(k)} f_{kj,s} \geq 1 - M\lambda_{r,s} \quad r \in \Omega_k \cap \Omega_{\mathrm{F}} \tag{10f}$$

$$0 \leq Z_{r,s} \leq \lambda_{r,s} \quad r \in \Omega_{\mathrm{F}} \tag{10g}$$

$$v_{i,t} - U_0^2 \geq -M\left(2 - Z_{i,s} - K_{t,s}\right) \quad i \in \Omega_{\mathrm{SOP}} \tag{10h}$$

where N_{Z} and N_{G} are the total numbers of outage regions and substations, respectively; $f_{ij,s}$, $f_{ik,s}$, and $f_{kj,s}$ are the fictitious flow variables of line ij, ik, and kj at stage s, respectively; and $\lambda_{r,s}$ is the binary variable indicating whether node r is a fictitious source node at stage s. The fictitious source nodes are used to ensure the radial operation of the ADN and have no actual physical meaning. If $\lambda_{r,s} = 1$, node r is the fictitious source node at stage s. Otherwise, node r is a regular node.

Equations (10a)-(10f) represent the radial constraints of ADN. Equation (10g) is considered to ensure that each region has one voltage-supported node at most after network reconfiguration. Besides, (1b) is modified as (10h) to adapt to the multi-stage supply restoration model.

Considering the limitation of (10a), one node from each region can be selected as the candidate fictitious source node. Ω_{F} is used to represent the set composed of the candidate fictitious source nodes. As a result, the number of binary variables $\lambda_{r,s}$ is reduced to the number of regions, decreasing the total number of binary variables. To ensure the reliable operation of the system, the nodes capable of providing voltage support are selected as candidate fictitious source nodes. If none of nodes in the region can provide voltage support, any node can be selected as the candidate fictitious source node. The detailed explanation of (10a) is shown in Supplementary Material A.

The DistFlow model is used to describe power flow constraints of ADN [34], which is expressed as:

$$\sum_{i \in \pi(j)} \left(P_{ij,t} - r_{ij} l_{ij,t}\right) + P_{j,t} = \sum_{g \in \xi(j)} P_{jg,t} \tag{11a}$$

$$\sum_{i \in \pi(j)} \left(Q_{ij,t} - x_{ij} l_{ij,t}\right) + Q_{j,t} = \sum_{g \in \xi(j)} Q_{jg,t} \tag{11b}$$

$$P_{j,t} = P_{j,t}^{\mathrm{DG}} + P_{j,t}^{\mathrm{SOP}} - R_{j,t} P_{j,t}^{\mathrm{LOAD}} \tag{11c}$$

$$Q_{j,t} = Q_{j,t}^{\mathrm{DG}} + Q_{j,t}^{\mathrm{SOP}} - R_{j,t} Q_{j,t}^{\mathrm{LOAD}} \tag{11d}$$

$$v_{i,t} - v_{j,t} + \left(r_{ij}^2 + x_{ij}^2\right) l_{ij,t} - 2\left(r_{ij} P_{ij,t} + x_{ij} Q_{ij,t}\right) + M\left(2 - s_{ij,s} - K_{t,s}\right) \geq 0 \quad \forall ij \in \Omega_{\mathrm{L}}^{\mathrm{sw}}, \forall t, s \tag{11e}$$

$$v_{i,t} - v_{j,t} + \left(r_{ij}^2 + x_{ij}^2\right) l_{ij,t} - 2\left(r_{ij} P_{ij,t} + x_{ij} Q_{ij,t}\right) - M\left(2 - s_{ij,s} - K_{t,s}\right) \leq 0 \quad \forall ij \in \Omega_{\mathrm{L}}^{\mathrm{sw}}, \forall t, s \tag{11f}$$

$$v_{i,t} - v_{j,t} + \left(r_{ij}^2 + x_{ij}^2\right) l_{ij,t} - 2\left(r_{ij} P_{ij,t} + x_{ij} Q_{ij,t}\right) = 0 \quad \forall ij \in \Omega_{\mathrm{L}} \backslash \left(\Omega_{\mathrm{L}}^{\mathrm{sw}} \cup \Omega_{\mathrm{L}}^{*}\right), \forall t, s \tag{11g}$$

$$-M\left(s_{ij,s} - 1 + K_{t,s}\right) \leq P_{ij,t} \leq M\left(s_{ij,s} + 1 - K_{t,s}\right) \quad \forall ij \in \Omega_{\mathrm{L}}^{\mathrm{sw}}, \forall t, s \tag{11h}$$

$$-M\left(s_{ij,s} - 1 + K_{t,s}\right) \leq Q_{ij,t} \leq M\left(s_{ij,s} + 1 - K_{t,s}\right) \quad \forall ij \in \Omega_{\mathrm{L}}^{\mathrm{sw}}, \forall t, s \tag{11i}$$

$$0 \le l_{ij,t} \le \left(I_{ij}^{\max}\right)^2 \left(s_{ij,s} + 1 - K_{t,s}\right) \quad \forall ij \in \Omega_{\mathrm{L}}^{\mathrm{sw}}, \forall t, s \tag{11j}$$

$$0 \le l_{ij,t} \le \left(I_{ij}^{\max}\right)^2 \quad \forall ij \in \Omega_{\mathrm{L}} \backslash \left(\Omega_{\mathrm{L}}^{\mathrm{sw}} \cup \Omega_{\mathrm{L}}^{*}\right), \forall t, s \tag{11k}$$

$$\left(V_i^{\min}\right)^2 \left(E_{k,s} - 1 + K_{t,s}\right) \le v_{i,t} \le \left(V_i^{\max}\right)^2 \left(E_{k,s} + 1 - K_{t,s}\right) \tag{11l}$$

$$\left\| \begin{bmatrix} 2P_{ij,t} & 2Q_{ij,t} & l_{ij,t} - v_{i,t} \end{bmatrix}^{\mathrm{T}} \right\|_2 \le l_{ij,t} + v_{i,t} \tag{11m}$$

where Ω_{L}^{*} is the set of faulty lines; $P_{ij,t}$ and $Q_{ij,t}$ are the active and reactive power flows of line ij in time interval t, respectively; $P_{i,t}^{\mathrm{DG}}$ and $Q_{i,t}^{\mathrm{DG}}$ are the active and reactive power outputs of DG at node i in time interval t, respectively; $R_{j,t}P_{j,t}^{\mathrm{LOAD}}$ and $R_{j,t}Q_{j,t}^{\mathrm{LOAD}}$ are the restored active and reactive power at node j in time interval t, respectively; x_{ij} is the reactance of line ij; $I_{ij}^{\max}$ is the maximum current of line ij; and $V_i^{\min}$ and $V_i^{\max}$ are the minimum and maximum voltages of node i, respectively.

Equations (11a) and (11b) indicate the active and reactive power balances at node j, respectively. In this paper, the direction of injecting power into the ADN is defined as the positive direction. Equations (11c) and (11d) represent the net active and reactive power at node j in time interval t, respectively. Equations (11e) and (11f) denote the line voltage drop between node i and node j by the big-M method, and do not work when the switch between node i and node j is disconnected. Equation (11g) represents the line voltage drop constraints in the normal lines. Equations (11h)-(11k) constrain the upper and lower limits of active/reactive power and current in line ij. Power and current are permitted only when the line ij is closed at stage s. For example, when $s_{ij,s}=1$ and $K_{t,s}=1$, $P_{ij,t}$ is not constrained. Similarly, the range of voltage magnitude is constrained by (11l). The capacity constraint of line ij is imposed using the second-order cone convex relaxation in (11m).

3) Load and DG Constraints

The load and DG constraints are given in (12a)-(12c).

$$0 \le R_{i,t} \le E_{k,s} + 1 - K_{t,s} \quad \forall i \in \Omega_k, \forall t, s \tag{12a}$$

$$P_{i,t}^{\mathrm{DG,ref}}\left(E_{k,s} - 1 + K_{t,s}\right) \le P_{i,t}^{\mathrm{DG}} \le P_{i,t}^{\mathrm{DG,ref}}\left(E_{k,s} + 1 - K_{t,s}\right) \tag{12b}$$

$$Q_{i,t}^{\mathrm{DG}} = \frac{P_{i,t}^{\mathrm{DG}}\sqrt{1-\kappa^2}}{\kappa} \tag{12c}$$

where $P_{i,t}^{\mathrm{DG,ref}}$ is the predicted active power generated by DG in time interval t; and κ is the power factor of DG.

The restoration ratios of nodes are constrained in (12a). Equations (12b) and (12c) represent the DG operation constraints. As shown in (12b), DGs can supply energy to ADN only when node i is energized at stage s.

4) Operation Constraints of SOP

The SOP operation constraints with MES integration are shown in (1a)-(3b). Equation (1a) is modified as (13) after stage division.

$$0 \le Z_{i,s} + Z_{j,s} \le 2 + \sum_{m \in \Omega_{\mathrm{M}}} \alpha_{n,m,t} - K_{t,s} \tag{13}$$

where $Z_{i,s}$ is the binary variable indicating whether the SOP terminal i provides voltage support at stage s.

5) Operation Constraints of MES

The operation constraints of MES are shown in (4a)-(5d). Thus, the proposed multi-stage supply restoration model can be expressed as (14), subject to (2a)-(8b), (10a)-(13).

$$\min f = f_{\mathrm{P}} + f_{\mathrm{L}} + f_{\mathrm{E}} + f_{\mathrm{S}} \tag{14}$$

The strategies of switch operation and selection of SOP control mode can be derived by solving the above model on the long timescale. The operation variables used to derive the lower-level restoration model are $s_{ij,s}$, $Z_{i,s}$, and $E_{k,s}$.

C. Coping with Uncertainty

Uncertainties of DGs and loads will affect the effectiveness of strategies. Thus, the uncertainty set $\mathbb{U}$ is established based on the typical scenarios to describe the uncertainties of DGs and loads, as shown in (15).

$$\mathbb{U} = \left\{ u : u_\omega = u_\omega^0 + \eta_\omega, \sum_{\omega=1}^{N_\omega} \eta_\omega = 0, \underline{\eta}_\omega \le \eta_\omega \le \bar{\eta}_\omega \right\} \tag{15}$$

where u is the element of the uncertainty set $\mathbb{U}$; N_ω is the number of scenarios; u_ω is the probability of scenario ω; u_ω^0 is the predicted probability of scenario ω; η_ω is the probability volatility coefficient in scenario ω; and $\bar{\eta}_\omega$ and $\underline{\eta}_\omega$ are the upper and lower limits of the volatility coefficient in scenario ω, respectively.

Based on the uncertainty set, a min-max bi-layer model is formulated in (16).

$$\min_{y^\omega \in \boldsymbol{Y}^\omega, z^\omega \in \boldsymbol{Z}^\omega} \left(\max_{u \in \mathbb{U}} \sum_{\omega=1}^{N_\omega} u_\omega f^\omega \right) \tag{16}$$

where $\boldsymbol{Y}^\omega$ and $\boldsymbol{Z}^\omega$ are the constraint sets of variables y^ω and z^ω, respectively; and f^ω is the objective function of scenario ω.

The model can be further linearized by duality theory [35], as shown in (17). Besides, the process of dual transformation is shown in Supplementary Material B.

$$\min \sum_{\omega=1}^{N_\omega} \left(u_\omega^0 \left(f^\omega\right) + \bar{\eta}_\omega \varsigma_\omega' + \underline{\eta}_\omega \varsigma_\omega'' \right) \tag{17a}$$

s.t.

$$z + \varsigma_\omega' + \varsigma_\omega'' = f^\omega \tag{17b}$$

$$\varsigma_\omega' \ge 0 \ge \varsigma_\omega'' \tag{17c}$$

$$\boldsymbol{A}\boldsymbol{x} \le \boldsymbol{b} \tag{17d}$$

$$\boldsymbol{B}\boldsymbol{g}^\omega \le \boldsymbol{c} \tag{17e}$$

$$\boldsymbol{C}\boldsymbol{g}^\omega + \boldsymbol{D}\boldsymbol{d}^\omega + \boldsymbol{E}\boldsymbol{x} = \boldsymbol{e}^\omega \tag{17f}$$

$$\left\| \boldsymbol{F}\boldsymbol{d}^\omega + \boldsymbol{G}\boldsymbol{g}^\omega + \boldsymbol{p} \right\|_2 \le \boldsymbol{f}^{\mathrm{T}}\boldsymbol{d}^\omega + \boldsymbol{h} \tag{17g}$$

where $\boldsymbol{A}$, $\boldsymbol{B}$, $\boldsymbol{C}$, $\boldsymbol{D}$, $\boldsymbol{E}$, $\boldsymbol{F}$, and $\boldsymbol{G}$ are the coefficient matrices of constraints; $\boldsymbol{b}$, $\boldsymbol{c}$, $\boldsymbol{e}$, $\boldsymbol{f}^{\mathrm{T}}$, $\boldsymbol{h}$, and $\boldsymbol{p}$ are constant column vectors; $\boldsymbol{d}^\omega$ is the set of fictitious flow variables and power flow variables in scenario ω; $\boldsymbol{x}$ is the binary variable vector for switch status and selection of SOP control mode; $\boldsymbol{g}^\omega$ is the set of variables related to SOPs, MESs, and DGs in scenario ω; and $\boldsymbol{e}^\omega$ is the load demand in scenario ω.

Equations (17a)-(17c) denote the dual constraints of (15). Equation (17d) represents the binary variable constraints re-

lated to switch and supply status in scenario ω. Equation (17e) indicates inequality constraints in scenario ω. Equation (17f) represents the equation constraints in scenario ω. Equation (17g) represents the second-order cone constraints in scenario ω.

Based on the uncertainty handling method, the uncertainties of DGs and loads in ADNs are modeled to enhance the effectiveness of the restoration method.

Note that the solution of multi-stage supply restoration model may be time-consuming. To ensure timely strategy determination in practice, the strategies of switch operation and selection of SOP control mode at stage 1 can be determined based only on the current system state. Subsequently, the multi-timescale strategies of the subsequent stages can be derived based on the results of stage 1.

IV. Rolling Correction Restoration Strategy at Lower Level

In this section, the rolling correction restoration strategy is proposed at the lower level. The restoration strategies of SOPs and MESs are corrected by dynamically updating the information of the transport network and ADN in each time interval.

A. Rolling Correction Restoration Strategy

The framework of the rolling correction restoration strategy is illustrated in Fig. 3. The correction horizon T_C is used to correct the restoration strategy of SOPs and MESs in current time internal. And T_P represents the prediction horizon. As shown in Fig. 3, the strategies of switch operation and selection of SOP control mode at the upper level are used to solve the restoration strategy on the short timescale. The power output of MES and SOP can be corrected at the lower level.

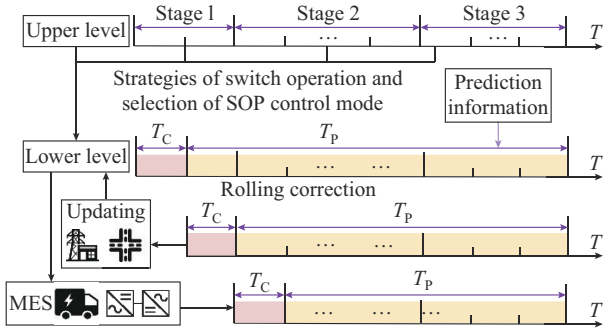

Fig. 3. Framework of rolling correction restoration strategy.

The restoration model for each rolling correction is shown in (18) without uncertainties, subject to (2a)-(6), (11a)-(12c). The operation variables required to be output are $P_{i,t}^{SOP}$, $Q_{i,t}^{SOP}$, $P_{n,m,t}$, $\alpha_{n,m,t}$, $\gamma_{m,t}$, and $E_{m,t}$.

$$\min f = f_P + f_L + f_E + f_S \tag{18}$$

Based on the switch status and SOP control mode derived from the upper level, the power transfer of flexible resources and the travelling route of MES can be timely obtained at the lower level.

However, the determined travelling route of MES cannot be easily changed during the correction horizon. To ensure the effectiveness of MES scheduling, the uncertainty within prediction horizon also needs to be resolved by (17), and $\boldsymbol{x}$ becomes the binary variable vector for the MES position.

B. Update of Information on Transport Networks Based on Virtual Traffic Node

The update of the transport network contains two aspects: the update of the current traffic conditions of each road and the update of the current MES positions. When the MES is travelling on the transport network, the current MES position cannot be obtained only by (5a)-(5d). Consequently, a virtual traffic node is introduced to represent the real-time MES position in mobility status, as shown in Fig. 4. Equation (19) is introduced for updating the MES position.

$$\delta_{m,t_P} = \begin{cases} \delta_m & t_P = 1 \\ \delta_{mv,t_P} & t_P > 1, \gamma_{m,t_P} = 1 \\ \delta_{m,t_P-1} & t_P > 1, \gamma_{m,t_P} = 0 \end{cases} \tag{19}$$

where t_P is the current rolling moment; δ_{m,t_P} is the current MES position; and δ_{mv,t_P} indicates that the MES is in a virtual node at current time interval.

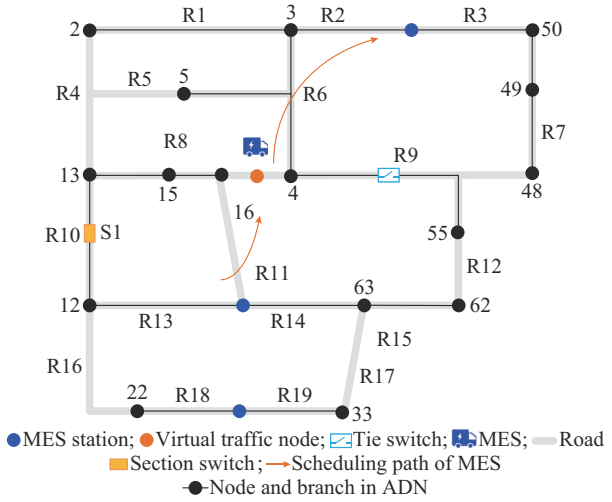

Fig. 4. Transport network with virtual traffic node.

Equation (19) indicates that the MES in mobility status is located at the virtual node; otherwise, the MES is located in the corresponding SOP. The travelling route and current MES position can be obtained by Dijkstra algorithm. The remaining time for the MES to travel to other SOPs can be calculated based on real-time traffic information. The MES scheduling strategy can be derived by (5a)-(5d) and (19).

The flowchart of the rolling correction restoration strategy considering the update of transport network is shown in Fig. 5, where T_H is the entire timescale of restoration.

Based on the updated information, the transport network matrix is calculated for MES travelling route selection. The scheduling strategies of SOPs and MESs can be rolling corrected by solving the restoration model in current time interval.

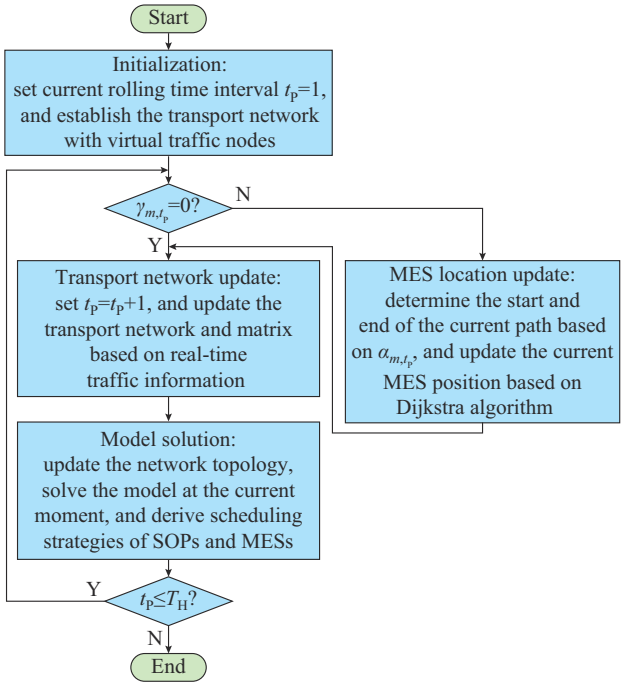

Fig. 5. Flowchart of rolling correction restoration strategy.

The proposed bi-level supply restoration model is a mixed-integer nonlinear programming (MINLP) model essentially, which is difficult to solve directly. Based on the second-order cone transformation and convex relaxation, the MINLP model is transformed into a mixed-integer second-order cone programming (MISOCP) model, which can be effectively solved by commercial solvers. Besides, the GAP is adopted to evaluate the accuracy of the result, as shown in (20). The model is considered to be solved exactly when the GAP value is close to 0 [36].

$$GAP = \left\| \left(v_{i,t} l_{ij,t} - P_{ij,t}^2 - Q_{ij,t}^2 \right) \Big/ \left(v_{i,t} l_{ij,t} \right) \right\|_\infty \tag{20}$$

V. Case Studies and Analysis

In this section, the effectiveness of the proposed bi-level supply restoration method is verified on a modified practical distribution network. The proposed method is implemented in the YALMIP optimization toolbox with MATLAB R2020b and solved by Gurobi 10.0.1. The numerical experiments are performed on a computer with an Intel Core i7-11700 CPU @ 2.50 GHz and 16 GB of RAM.

A. Modified Practical Distribution Network

The structure of the modified practical distribution network along with the transport network is shown in Fig. 6. The rated voltage level is 11.4 kV. The total active and reactive power demands are 22.31 MW and 16.39 Mvar, respectively. Manually controlled switches require 30 min to operate and are labeled with "*". The remotely controlled switches require 0.5 min to operate. The unit price of power loss c_P is set to be 30 $/kWh, and the unit price of power purchased from the upper network c_L is 0.076 $/kWh. The cost associated with the change in switch operation c_S is set to be $1 per time.

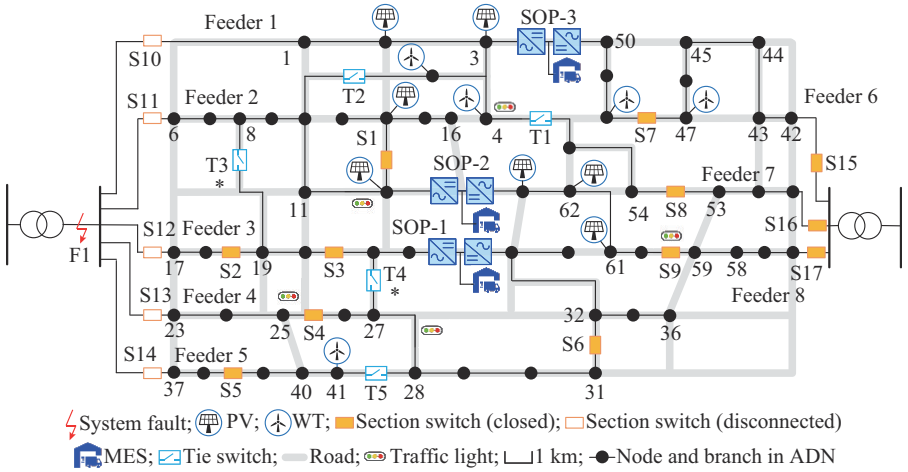

Fig. 6. Structure of modified practical distribution network with transport network.

The photovoltaic (PV) units and wind turbines (WTs) are integrated into the modified practical distribution network separately. The power factor of DG is set to be 1.0, and the specific information is shown in Table II. Besides, nodes 21, 22, 33, and 34 are commercial loads, and the remaining nodes are residential loads.

To consider the impact of the uncertainties of the DGs and loads, 1000 scenarios are generated based on normal state, and three typical scenarios are obtained via clustering. The predicted DG and load prediction output curves are given in Fig. SC1 of Supplementary Material C.

TABLE II
Parameter of DG Installation

Type	Node	Capacity
WT	4, 5, 41, 47, 48	800 kVA
PV	2, 3, 12, 13, 61, 62, 63	600 kWp

In addition, three SOPs are installed in the distribution network. The capacity of each terminal is set to be 3.5 MVA with a loss coefficient of 0.01, and MES can be integrated with SOP through the DC link. The maximum MES charg-

ing or discharging power is 1 MW with a capacity of 1 MWh. The upper and lower limits of SOCs are designed to be 95% and 20%, respectively, and the initial SOC is set to be 60%. It is assumed that MES consumes 0.75 kWh of electricity per unit time interval while travelling.

Part of the traffic network in Fig. 6 is selected for modeling according to SOPs with MES integration points. The topology of the transport network is shown in Fig. 4. The travelling time among SOPs is depicted in Fig. SC2 of Supplementary Material C.

Assuming that a fault occurs in the main transformer on the left side, the fault restoration time is from 10: 00 to 14:00, and nodes 1-41 are de-energized. After the fault occurs, switches S10-S14 are opened to isolate the fault.

B. Result Analysis

The proposed bi-level supply restoration method is conducted to minimize the outage loss during the restoration process.

1) Supply Restoration of ADN

The restoration of multiple resources is analyzed based on the proposed bi-level supply restoration method. The diagram of restoration configuration in outage regions is presented in Fig. 7. The terminal of SOP at the green node adopts the $U_{ac}\theta$ control mode. As shown in Fig. 7, T5 is closed to transfer energy from WT in node 41 to Feeders 3 and 4 at stage 1. With MES integration, both terminals of SOP-1 adopt $U_{ac}\theta$ control mode to ensure high-quality restoration. After that, T3 and T4 are further operated at stage 2 to ensure the restoration from Feeders 3-5. Meanwhile, the control modes of SOP2 and SOP3 are optimized to improve the restoration efficiency.

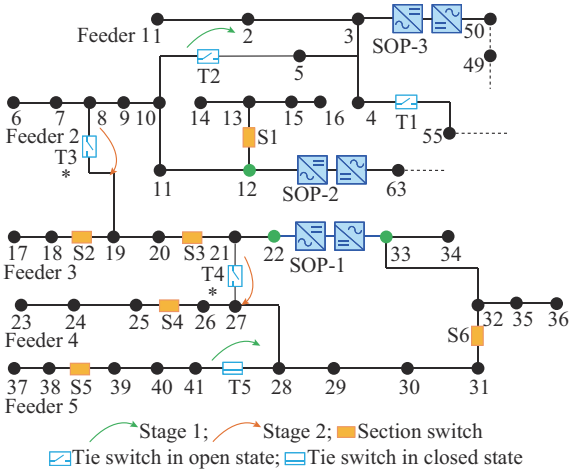

Fig. 7. Restoration configuration in outage regions.

Note that nodes 22 and 33 are connected through SOP to enable the flexible interconnection between Feeders 3 and 4. Considering the flexibility of the SOP, the loop structure formed by the SOP is permitted in distribution networks. Therefore, the topology illustrated in Fig. 7 meets the radial operation requirements of distribution networks.

Figure 8 shows the supply restoration for SOPs. SOP-22 indicates the active power output of the SOP terminal located at node 22. If positive, the power is transferred from SOP terminal to node 22. As can be observed in Fig. 6, SOP-1 consists of SOP-22 and SOP-33, and so on. SOP-1 transfers power to both outage regions from MES. Due to the delay of manually controlled switches, excess energy from DGs cannot be consumed locally. SOP-2 and SOP-3 transfer power to Feeders 6 and 7 to balance the feeder loads. After 10: 30, Feeders 3-5 are energized through T3 and T4. SOP-1-SOP-3 transfer energy to the outage regions to improve the supply restoration ratio of ADN.

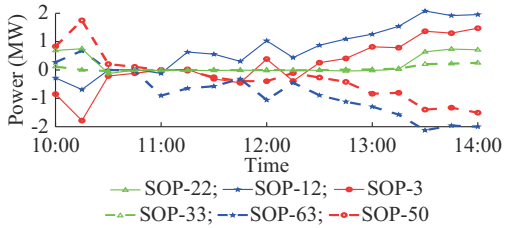

Fig. 8. Supply restoration for SOPs.

Figure 9 shows the supply restoration of MES. The MES integrates with the DC link of SOP-1 from 10:00 to 10:45 to provide power support for the outage regions. Afterward, MES travels to SOP-2 and SOP-3 to store energy from DGs. Finally, MES returns to SOP-1 to provide power to the nodes located at the edge of the ADN. Power complementarity is realized in the spatial and temporal dimensions.

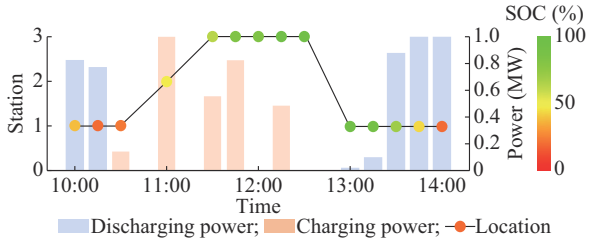

Fig. 9. Supply restoration of MESs.

The relaxation deviation value is shown in Fig. SC3 of Supplementary Material C, and the error is within tolerance. The model has been exactly solved.

2) Comparison of Restoration Performance

The following three schemes are used to verify the effectiveness of the proposed supply restoration method.

1) Scheme I: single-stage supply restoration method is conducted without multi-stage restoration of ADN.

2) Scheme II: multi-stage supply restoration model adopted in [29] is conducted.

3) Scheme III: the proposed bi-level supply restoration method for ADN is conducted.

The operation costs of the three schemes are detailed in Table III. As can be observed, a significant load loss is evident in Scheme I, with the total operation cost nearly 18 times higher than that of Scheme III. Compared with Scheme I, the restoration cost in Scheme II is greatly reduced. However, there are still serious load loss. In Scheme III, the load restored cost is reduced by nearly 85%, verifying the effectiveness of the proposed method.

The restoration ratios and operation strategies of SOP at

different stages are shown in Table IV. It can be observed that the restoration ratios between 10:00 and 10:30 are generally low for all three schemes. The manually controlled switches T3 and T4 cannot operate in time, resulting in a severe load loss on Feeders 3-5. In addition, the restoration ratios increase by more than 30% in Scheme II by multi-stage supply restoration model after 10:30. Nevertheless, the restoration ratio has not reached 100% at stage 2 because of the fluctuations of DGs and loads. Compared with Scheme II, Scheme III achieves 100% load restoration at stage 2 by rolling correction of MES and SOP scheduling strategies.

TABLE III
OPERATION COSTS OF THREE SCHEMES

Scheme	Total cost ($)	Unrestored load cost ($)	Operation power loss cost ($)	MES loss cost ($)	SOP loss cost ($)	Switch action cost ($)
I	431994.52	431964.60	11.38	0.30	17.24	1
II	160368.90	160318.26	23.19	1.67	21.78	4
III	24232.80	24178.72	29.60	1.62	18.86	4

TABLE IV
RESTORATION RATIOS AND OPERATION STRATEGIES OF SOP AT DIFFERENT STAGES

Scheme	Stage	Restoration ratio (%)	Operation strategy
I	1 (10:00-14:00)	48.76	1) Close T5. 2) Terminals at both ends of the SOP-1 adopt $U_{ac}\theta$ control mode. 3) SOP-2 and SOP-3 adopt $U_{ac}\theta$-$U_{dc}Q$ control mode.
II	1 (10:00-10:30)	63.53	1) Close T2 and T5. 2) Terminals at both ends of SOP-1 adopt $U_{ac}\theta$ control mode. 3) SOP-2 adopts $U_{ac}\theta$-$U_{dc}Q$ control mode. 4) SOP-3 adopts PQ-$U_{dc}Q$ control mode.
	2 (10:31-14:00)	82.92	1) Close T3 and T4. 2) Terminal at node 22 adopts $U_{dc}Q$ control mode and terminal at node 33 adopts $U_{ac}\theta$ control mode 3) SOP-2 and SOP-3 adopt PQ-$U_{dc}Q$ control mode.
III	1 (10:00-10:30)	70.58	1) Close T2 and T5. 2) Terminals at both ends of SOP-1 adopt $U_{ac}\theta$ control mode. 3) SOP-2 adopts $U_{ac}\theta$-$U_{dc}Q$ control mode. 4) SOP-3 adopts PQ-$U_{dc}Q$ control mode.
	2:(10:31-14:00)	100.00	1) Close T3 and T4. 2) Terminal at node 22 adopts $U_{dc}Q$ control mode and terminal at node 33 adopts $U_{ac}\theta$ control mode. 3) SOP-2 and SOP-3 adopt PQ-$U_{dc}Q$ control mode.

The specific node restoration ratios of the above three schemes in fault regions are shown in Figs. 10-12. The restoration ratio of the entire distribution network is generally low in Scheme I, with a certain percentage of nodes exhibiting a restoration ratio of less than 50%. As the coordination with manually controlled switches is considered in Scheme II, the restoration ratio is improved to some extent. In Scheme III, the restoration ratio at each node is greatly improved by rolling correction.

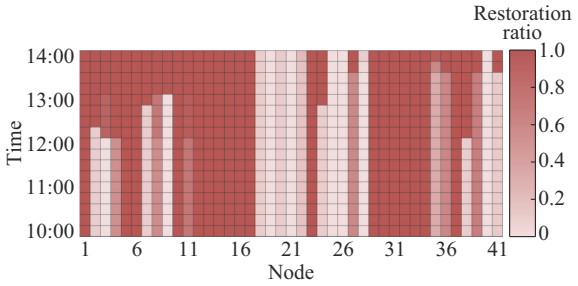

Fig. 10. Restoration ratio of nodes in Scheme I.

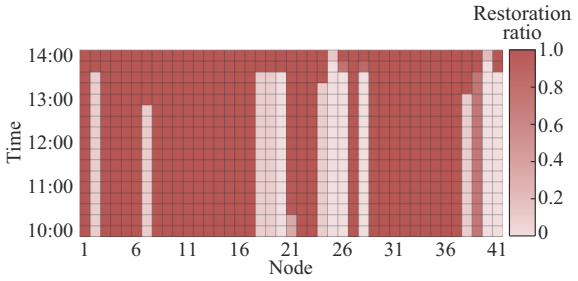

Fig. 11. Restoration ratio of nodes in Scheme II.

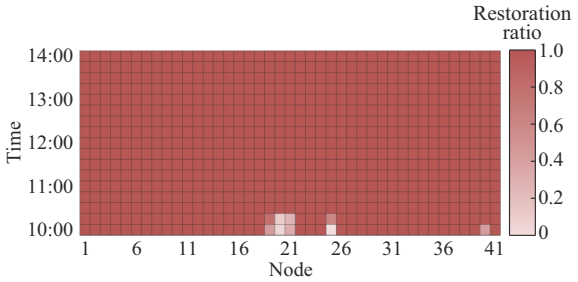

Fig. 12. Restoration ratio of nodes in Scheme III.

The restoration strategies for SOPs and MESs in Scheme I and Scheme II are given in Figs. SC4-SC7 of Supplementary Material C, respectively. The above results show that the proposed bi-level supply restoration method reduces the impact of uncertainty and improves supply restoration efficiency.

3) Analysis of Computation Performance

Table V shows the computation performance of the three schemes.

TABLE V
COMPUTATION PERFORMANCE OF THREE SCHEMES

Scheme	Level	Computation time (s)
I		13.09
II		37.56
III	Upper level	93.30
	Lower level	38.65

The computation time of Scheme I is the shortest. However, the strategies derived from Scheme I ignore the sequen-

tial coordination of multiple resources in ADN, where a serious loss of load is exhibited. The sequential coordination of multiple resources at different timescales is realized in Scheme II, and the capability of restoration is greatly improved by the multi-stage supply restoration model. Nevertheless, there are more binary variables and related constraints, and the solution time is about half a minute.

Scheme III adopts the proposed bi-level supply restoration method. At the upper level, the multi-stage action strategies for switches on the long timescale are derived. Due to the consideration of the uncertainties, the solution of the multi-stage supply restoration model is time-consuming. Thus, the initial strategies of switch operation and selection of SOP control mode at stage 1 are determined only based on the current system state, and the computation time of stage 1 is 1.05 s. The duration of stage 1 is 30 min. The solution time for the switch operation and selection of SOP control mode at stage 2 is 92.25 s, which is within 30 min, ensuring the timely determination of strategies at stage 2.

At the lower level, the rolling correction restoration strategy is proposed to adapt to DG and load fluctuations and varied traffic conditions, and the rolling optimization interval is set to be 15 min. Besides, the mean computation time for each rolling optimization is approximately half a minute, which fulfills the requirements in practice.

C. Scalability Verification

The proposed bi-level supply restoration method is further implemented on the modified IEEE 123-node distribution network in Fig. 13 to verify the scalability. Nodes 36-52, 77, 78, 87-97, 102-115, 117, 120, and 123 are characterized as commercial loads, and the remaining nodes are characterized as residential loads. The traffic network is also shown in Fig. 13, and the travelling time among SOPs is depicted in Fig. SD1 of Supplementary Material D. Other parameters are the same as the test case in Fig. 6. Assuming that a fault occurs in line 9-14, and the fault time is from 14: 00 to 18:00.

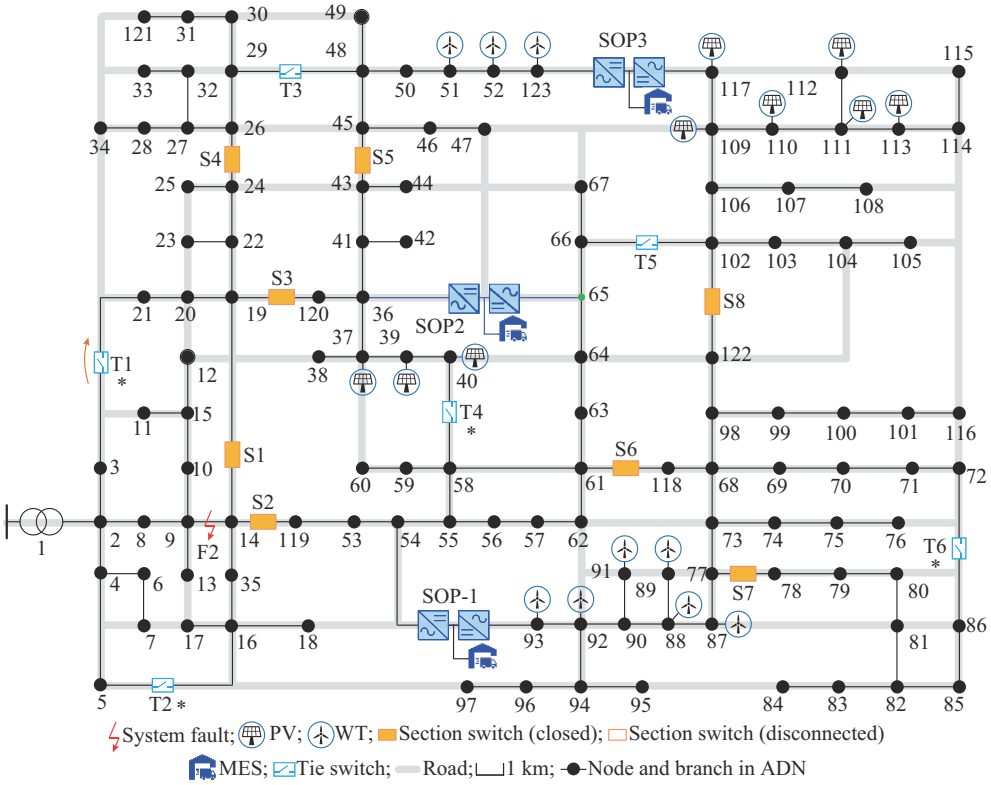

Fig. 13. Structure of modified IEEE 123-node distribution network.

According to the optimization results, the duration of stage 1 is from 14:00 to 14:30, and the duration of stage 2 is from 14:31 to 18:00. The strategies of switch operation and selection of SOP control mode are also shown in Fig. 13. The terminal of SOP at node 65 adopts $U_{ac}\theta$ control model at stage 1. The orange arrow represents that the switch T1 is closed at stage 2 to transfer power to the outage regions. The restoration strategies for SOPs and MESs are shown in Figs. SD2 and SD3 of Supplementary Material D.

Table VI presents the operation costs of the three schemes in the modified IEEE 123-node distribution network. The power restoration cost in Scheme II is approximately 10 times lower than that in Scheme I. Considering the uncertainties of DGs and loads, the supply restoration ratio is further improved in Scheme III.

As for the computation performance in IEEE 123-node distribution network, the computation time of the restoration strategies at stage 1 is less than 3 s at the upper level. As the scale of the test case expands, the number of related variables increases, resulting in longer computation time. The computation time of stage 2 is approximately 331 s, which also ensures the timely implementation of the strategy.

TABLE VI
OPERATING COSTS OF THREE SCHEMES IN MODIFIED IEEE 123-NODE DISTRIBUTION NETWORK

Scheme	Total cost ($)	Unrestored load cost ($)	Operation power loss cost ($)	MES loss cost ($)	SOP loss cost ($)	Switch action cost ($)
I	9276.21	9238.75	27.00	3.34	6.12	1
II	942.67	886.80	43.34	1.18	10.35	1
III	422.99	369.40	41.33	1.18	10.08	1

At the lower level, the mean computation time for each rolling optimization is approximately 1.5 min. The lower-level model includes binary variables only related to the MES, and the computation time is less affected by the scales of ADNs. Hence, the computation time grows approximately linearly.

In summary, the solution time of the proposed method can meet the practical application and improve the performance of supply restoration.

VI. CONCLUSION

This paper proposes a bi-level supply restoration method for ADNs considering multi-resource coordination. As validated in test cases, the SOP restoration with MES integration achieves the coordination of SOP and MES in spatial and temporal dimensions. At the upper level, the multi-stage supply restoration model can derive the reliable switch and SOP control method on the long timescale. At the lower level, the rolling correction restoration strategy responds to the fluctuations of loads and DGs on the short timescale. The proposed method fully explores the potential of multiple resources for ADN restoration and further improves the restoration efficiency of ADN.

Several directions can be outlined for future research. The efficiency of supply restoration in distribution networks is affected by the positions and capacity of MESs and SOPs, so it is important to realize the coordinated planning of MESs and SOPs. In addition, considering the uncertainties from the fault locations and the SOC of MES, the uncertainty model will be further studied to enhance the effectiveness of the restoration method. Moreover, supply restoration based on data-driven methods should be further investigated.

REFERENCES

[1] A. Bosisio, A. Berizzi, D. Lupis *et al.*, "A tabu-search-based algorithm for distribution network restoration to improve reliability and resiliency," *Journal of Modern Power Systems and Clean Energy*, vol. 11, no. 1, pp. 302-311, Jan. 2023.

[2] Q. Zhao, W. Liao, S. Wang *et al.*, "Robust voltage control considering uncertainties of renewable energies and loads via improved generative adversarial network," *Journal of Modern Power Systems and Clean Energy*, vol. 8, no. 6, pp. 1104-1114, Nov. 2020.

[3] J. Zhao, Z. Zhang, H. Yu *et al.*, "Cloud-edge collaboration-based local voltage control for DGs with privacy preservation," *IEEE Transactions on Industrial Informatics*, vol. 19, no. 1, pp. 98-108, Jan. 2023.

[4] X. Yang, C. Xu, J. Wen *et al.*, "Cooperative repair scheduling and service restoration for distribution systems with soft open points," *IEEE Transactions on Smart Grid*, vol. 14, no. 3, pp. 1827-1842, May 2023.

[5] A. Azizi, B. Vahidi, and A. F. Nematollahi, "Reconfiguration of active distribution networks equipped with soft open points considering protection constraints," *Journal of Modern Power Systems and Clean Energy*, vol. 11, no. 1, pp. 212-222, Jan. 2023.

[6] A. Tao, N. Zhou, Y. Chi *et al.*, "Multi-stage coordinated robust optimization for soft open point allocation in active distribution networks with PV," *Journal of Modern Power Systems and Clean Energy*, vol. 11, no. 5, pp. 1553-1563, Sept. 2023.

[7] C. Wang, J. Sun, M. Huang *et al.*, "Two-stage optimization for active distribution systems based on operating ranges of soft open points and energy storage system," *Journal of Modern Power Systems and Clean Energy*, vol. 11, no. 1, pp. 66-79, Jan. 2023.

[8] Z. Yin, S. Wang, and Q. Zhao, "Sequential reconfiguration of unbalanced distribution network with soft open points based on deep reinforcement learning," *Journal of Modern Power Systems and Clean Energy*, vol. 11, no. 1, pp. 107-119, Jan. 2023.

[9] W. Liu, M. Fu, M. Yang *et al.*, "A bi-level Interval robust optimization model for service restoration in flexible distribution networks," *IEEE Transactions on Power Systems*, vol. 36, no. 3, pp. 1843-1855, May 2021.

[10] P. Li, J. Ji, H. Ji *et al.,* "Self-healing oriented supply restoration method based on the coordination of multiple SOPs in active distribution networks," *Energy*, vol. 195, p. 116968, Mar. 2020.

[11] T. Zhang, X. Yu, Y. Mu *et al.*, "Multiple sources restoration for soft open points in distribution networks with a two-stage accelerated algorithm," *IEEE Transactions on Sustainable Energy*, vol. 14, no. 2, pp. 892-905, Apr. 2023.

[12] J. Zhao, J. Qu, H. Ji *et al.*, "Robust operation of flexible distribution network with large-scale EV charging loads," *IEEE Transactions on Transportation Electrification*, vol. 10, no. 1, pp. 2207-2219, Mar. 2024.

[13] S. Zhang, Y. Fang, H. Zhang *et al.*, "Maximum hosting capacity of photovoltaic generation in SOP-based power distribution network integrated with electric vehicles," *IEEE Transactions on Industrial Informatics*, vol. 18, no. 11, pp. 8213-8224, Nov. 2022.

[14] C. Wang, J. Sun, M. Huang *et al.*, "Two-stage optimization for active distribution systems based on operating ranges of soft open points and energy storage system," *Journal of Modern Power Systems and Clean Energy*, vol. 11, no. 1, pp. 66-79, Jan. 2023.

[15] W. Sun, W. Liu, J. Zhang *et al*., "Bi-level optimal operation model of mobile energy storage system in coupled transportation-power networks," *Journal of Modern Power Systems and Clean Energy*, vol. 10, no. 6, pp. 1725-1737, Nov. 2022.

[16] Z. Wang, Q. Shi, K. Fan *et al.*, "Analytical modeling of disaster-induced load loss for preventive allocation of mobile power sources in urban power networks," *Journal of Modern Power Systems and Clean Energy*, vol. 12, no. 4, pp. 1063-1073, Jul. 2024.

[17] K. Lai and L. Zhang, "Sizing and siting of energy storage systems in a military-based vehicle-to-grid microgrid," *IEEE Transactions on Industry Applications*, vol. 57, no. 3, pp. 1909-1919, May-Jun. 2021.

[18] M. A. Masrur, A. G. Skowronska, J. Hancock *et al.*, "Military-based vehicle-to-grid and vehicle-to-vehicle microgrid – system architecture and implementation," *IEEE Transactions on Transportation Electrification*, vol. 4, no. 1, pp. 157-171, Mar. 2018.

[19] X. Jiang, J. Chen, W. Zhang *et al.*, "Two-step optimal allocation of stationary and mobile energy storage systems in resilient distribution networks," *Journal of Modern Power Systems and Clean Energy*, vol. 9, no. 4, pp. 788-799, Jul. 2021.

[20] Z. Lu, X. Xu, Z. Yan *et al.*, "Multistage robust optimization of routing and scheduling of mobile energy storage in coupled transportation and power distribution networks," *IEEE Transactions on Transportation Electrification*, vol. 8, no. 2, pp. 2583-2594, Jun. 2022.

[21] S. Yao, P. Wang, X. Liu *et al.*, "Rolling optimization of mobile energy storage fleets for resilient service restoration," *IEEE Transactions on Smart Grid*, vol. 11, no. 2, pp. 1030-1043, Mar. 2020.

[22] S. Lei, C. Chen, Y. Li *et al.*, "Resilient disaster recovery logistics of distribution systems: co-optimize service restoration with repair crew and mobile power source dispatch," *IEEE Transactions on Smart Grid*, vol. 10, no. 6, pp. 6187-6202, Nov. 2019.

[23] Y. Wang, Y. Xu, J. He *et al.*, "Coordinating multiple sources for service restoration to enhance resilience of distribution systems," *IEEE Transactions on Smart Grid*, vol. 10, no. 5, pp. 5781-5793, Sept. 2019.

[24] J. Liu, Z. Jiao, C. Zhang *et al.*, "Joint scheme for electric locomotive evacuation and distribution system restoration with faults of external power supply systems," *IEEE Transactions on Transportation Electrification*, vol. 10, no. 2, pp. 4252-4267, Jun. 2024.

[25] L. Zhang, C. Wang, J. Liang *et al.*, "A coordinated restoration method of hybrid AC/DC distribution network for resilience enhancement," *IEEE Transactions on Smart Grid*, vol. 14, no. 1, pp. 112-125, Jan.

2023.
[26] B. Chen, Z. Ye, C. Chen *et al.*, "Toward a synthetic model for distribution system restoration and crew dispatch," *IEEE Transactions on Power Systems*, vol. 34, no. 3, pp. 2228-2239, May 2019.
[27] B. Chen, Z. Ye, C. Chen *et al.*, "Toward a MILP modeling framework for distribution system restoration," *IEEE Transactions on Power Systems*, vol. 34, no. 3, pp. 1749-1760, May 2019.
[28] H. Sekhavatmanesh and R. Cherkaoui, "A multi-step reconfiguration model for active distribution network restoration integrating DG start-up sequences," *IEEE Transactions on Sustainable Energy*, vol. 11, no. 4, pp. 2879-2888, Oct. 2020.
[29] J. Jian, P. Ji, H. Yu *et al.*, "Multi-stage supply restoration of active distribution networks with SOP integration," *Sustainable Energy, Grids and Networks*, vol. 29, p. 100562, Mar. 2022.
[30] F. Fan, R. Zhang, Y. Xu *et al.*, "Robustly coordinated operation of an emission-free microgrid with hybrid hydrogen-battery energy storage," *CSEE Journal of Power and Energy Systems*, vol. 8, no. 2, pp. 369-379, Mar. 2022.
[31] X. Wang, Q. Guo, C. Tu *et al.*, "A two-layer control strategy for soft open points considering the economical operation area of transformers in active distribution networks," *IEEE Transactions on Sustainable Energy*, vol. 13, no. 4, pp. 2184-2195, Oct. 2022.
[32] S. Lei, C. Chen, H. Zhou *et al.*, "Routing and scheduling of mobile power sources for distribution system resilience enhancement," *IEEE Transactions on Smart Grid*, vol. 10, no. 5, pp. 5650-5662, Sept. 2019.
[33] Y. Yang, W. Yang, H. Yang *et al*., "Electrolyte design principles for low-temperature lithium-ion batteries," *eScience*, vol. 3, no. 6, p. 100170, Dec. 2023.
[34] J. Jian, J. Zhao, H. Ji *et al.*, "Supply restoration of data centers in flexible distribution networks with spatial-temporal regulation," *IEEE Transactions on Smart Grid*, vol. 15, no. 1, pp. 340-354, Jan. 2024.
[35] R. Jabr, "Segregated linear decision rules for inverter watt-var control," *IEEE Transactions on Power Systems*, vol. 36, no. 3, pp. 2702-2708, May 2021.
[36] R. Wang, H. Ji, P. Li *et al.*, "Multi-resource dynamic coordinated planning of flexible distribution network," *Nature Communications*, vol. 15, no. 1, p. 4576, May 2024.

Guanyu Song received the B.S. and Ph.D. degrees in electrical engineering from Tianjin University, Tianjin, China, in 2012 and 2017, respectively. He is currently a Senior Engineer with the School of Electrical and Information Engineering, Tianjin University. His current research interests include distributed generation system, and optimal planning and operation of smart distribution system.

Chiyuan Ma received the B.S. degree in electrical engineering from Tianjin University, Tianjin, China, in 2022. He is currently working toward the M.S. degree in electrical engineering with Tianjin University. His current research interests include optimal operation of distribution network.

Haoran Ji received the B. S. and Ph. D. degrees in electrical engineering from Tianjin University, Tianjin, China, in 2014 and 2019, respectively. From 2019 to 2021, he was a Postdoctoral Research with Tianjin University. He is currently an Associate Professor with Tianjin University. His research interests include distributed generation system and optimal operation of distribution network.

Hany M. Hasanien received the B.S., M.S., and Ph.D. degrees in electrical engineering from the Faculty of Engineering, Ain Shams University, Cairo, Egypt, in 1999, 2004, and 2007, respectively. Currently, he is Professor at the Electrical Power and Machines Department, Faculty of Engineering, Ain Shams University, and he is also with Future University in Egypt, Cairo, Egypt. His research interests include modern control, power system dynamics and control, energy storage system, renewable energy system, and smart grid.

Jiancheng Yu received the M.S. and Ph.D. degrees in electrical engineering from Tianjin University, Tianjin, China, in 2003 and 2006, respectively. He is the Senior Engineer (Professor level) of State Grid Tianjin Electric Power Company, Tianjin, China. His research interests include distribution network planning, distributed power supply, and smart power distribution and consumption.

Jinli Zhao received the Ph.D. degree in electrical engineering from Tianjin University, Tianjin, China, in 2007. She is currently an Associate Professor in the School of Electrical and Information Engineering, Tianjin University. Her research interests include operation and planning of distribution network, and power system security and stability.

Hao Yu received the B.S. and Ph.D. degrees in electrical engineering from Tianjin University, Tianjin, China, in 2010 and 2015, respectively. He is currently an Associate Professor with the School of Electrical and Information Engineering, Tianjin University. His current research interests include operation analysis and optimization of active distribution network and integrated energy system.

Peng Li received the B.S. and Ph.D. degrees in electrical engineering from Tianjin University, Tianjin, China, in 2004 and 2010, respectively. He is currently a Professor with the School of Electrical and Information Engineering, Tianjin University. His current research interests include operation and planning of active distribution network, modeling, and transient simulation of power system.